https://ieeexplore.ieee.org/document/7533923

Mobile Robot 6D Pose Estimation Using a Wireless Localization Network

Yassen Dobrev[1], Christoph Reustle[1], Tatiana Pavlenko[1], Florian Cordes[2], Martin Vossiek[1]
[1]Institute of Microwaves and Photonics (LHFT), Friedrich-Alexander-Universität Erlangen-Nürnberg (FAU), Erlangen, Germany
[2]Robotics Innovation Center, DFKI GmbH, Bremen, Germany
E-mail: yassen.dobrev@fau.de

***Abstract*—Global navigation satellite systems (GNSS) are widely used for localization on Earth, but are not available on other planets, so that robotic planetary exploration missions need to use alternative methods for localization. This paper presents a wireless localization network (WLN) for estimating the 3D position and 3D orientation of a mobile robot. It consists of at least one reference 24 GHz radar node with known pose, and a mobile node on the robot. The reference nodes can determine the distance and both spatial angles to the mobile robot (thus locating it in 3D) using round-trip time of flight measurements and digital beamforming. We use an extended Kalman filter (EKF) to fuse these results with the readings from the mobile node, and an inclinometer to determine the complete 6D pose of the mobile robot. Measurements in a realistic scenario prove the feasibility of the proposed concept.**

Keywords—wireless localization; 6D pose estimation; secondary radar; sensor fusion

I. Introduction

While global navigation satellite systems (GNSS) are widely used for localization on Earth, such systems are absent on other planets, so that robotic planetary exploration missions cannot rely on them for localization. An overview of currently employed alternatives based on relative sensors such as wheel encoders or visual odometry is given in [1]. The inherent drawback of such techniques is error accumulation, which leads to deterioration of the localization result as the mobile robot moves.

A typical exploration scenario includes the mapping of a crater wall by driving around it and taking a series of images as described in [1]. The images are combined to an integrated map and points of interest (POI) for closer study are identified in the map after the localization errors have been (manually) compensated. The mobile robot then returns to the POI locations for investigation. However, it can only accurately drive back to a POI if both the mobile robot and the target location are known.

We present a wireless localization network (WLN) for 6D pose estimation of mobile robots using sparse infrastructure. It consists of at least one reference node installed at the test site and another node on the mobile robot as depicted in Fig. 1. The WLN can improve and speed up the process of mapping and target finding in planetary exploration missions. It can also be used in terrestrial applications in places where GNSS is not available (e.g. indoors) or when higher accuracy or 3D orientation is required in a specified area.

This study was partly financially supported by the German Space Agency (DLR) under the project frames "TransTerrA", registration no. 50RA1301, "SOKOROB", registration no. 50RA1205, "LAOLa", registration no. 50NA1528 and by the Federal Ministry of Education and Research of Germany (BMBF) under the project frame "iserveU", registration no. 01IM12008F.

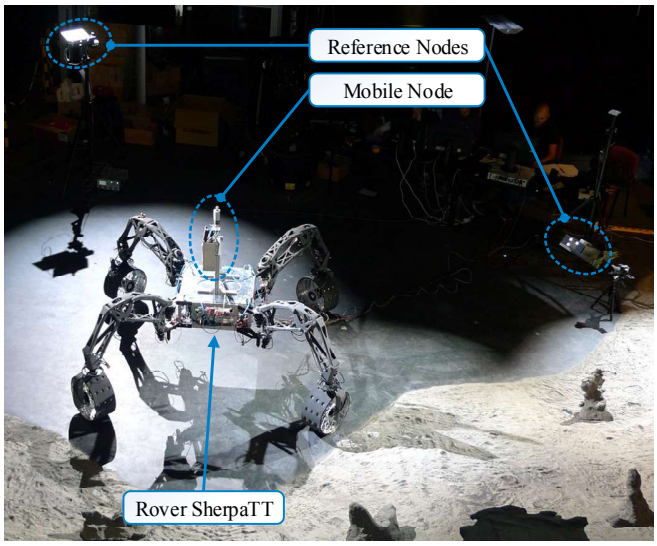

Fig. 1. The rover SherpaTT with WLN in the DFKI space exploration hall in Bremen, Germany.

II. Application Scenario

A. Application

The WLN is developed with the scope of the TransTerrA project [2]. The application scenario comprises multiple mobile robots cooperating in a mission on the lunar south pole. An exploration rover (SherpaTT, Fig. 1) is envisioned for wide range exploration of the area. It will take soil samples, carry modular payload items and so-called BaseCamps that serve as communication relays and sample container depots. A smaller and more agile rover is used as a shuttle to pick up deployed samples and transport them to the landing site for further inspection or transfer into a return stage to Earth. Additionally, the shuttle can transport battery modules in order to extend the runtime of the exploration rover. The mission scenario includes several rendezvous between exploration rover, shuttle, and BaseCamps. The WLN can be used to improve the localization of the mobile and immobile systems.

B. Expandable Rover for Planetary Applications

The experiments presented in this paper are based on an early integration study of the exploration rover SherpaTT. SherpaTT is a hybrid wheeled-leg rover with an active suspension system composed of four limbs with a wheel mounted at the end of each limb. A total of 20 active degrees of freedom (DoF) allow the robot to adapt to rough terrain while at the same time maintaining a desired body height and/or attitude of the central body. The robot will be equipped with a manipulator in the final integration stage. This will allow it to handle modular payloads that can be transported to four payload bays situated around the manipulator. SherpaTT will cooperate with the second mobile robot, Coyote III, in the final mission scenario [2]. The radar node is mounted on top of the central body for the experiments. More details on the system design of SherpaTT are available in [3].

III. Sensors

The WLN consists of two or more radar nodes. Each node is a single input multiple output (SIMO) frequency-modulated continuous-wave (FMCW) secondary radar with a center frequency of 24.125 GHz and a bandwidth of 250 MHz. The distance between two nodes is determined by the round-trip time of flight (RTOF) measurement principle using FMCW ramps, as described in [4]. Each device has 1 Tx and 8 Rx channels suitable for digital beamforming. All nodes have identical hardware, but run different software; they are equipped with different antenna arrays depending on their role in the network. A description of the previous hardware generation based on the same principles can be found in [5]. Our proposed WLN has the advantage of higher reliability and lower infrastructure cost over state-of-the-art wireless local positioning techniques based on TDOA / TOA / RTOF [6], since only a single measurement by a single reference node is needed for localizing the target in 3D.

A. Reference Node with Planar Antenna Array

The reference nodes are equipped with sparse planar antenna arrays. Each array comprises 8 patch antennas in an optimized 2D arrangement, which enables both azimuth and elevation angles of arrival of the received signal to be estimated. The array has a sidelobe level (SLL) of −3.7 dB, and a main beam width (MBW) of approximately 10° at broadside direction; its aperture size is 70×47 mm. We connect the array to the radar node and apply a calibration procedure as described in [7]. We found the unambiguous measurement range to be more than ±45° in both azimuth and elevation angles using the delay-and-sum beamformer in a series of measurements in an office-building foyer. We can estimate the 3D position of the mobile node relative to a reference node by combining the measured angles with the measured distance.

B. Mobile Node with Ring Antenna Array

The reference nodes are situated around the installation site and need to only cover the area in front of them, i.e., in a ±45° in azimuth and elevation, while the mobile node can be moved and rotated freely in the measurement site. Therefore, it needs a 360° range in azimuth and ±45° range in elevation for complete coverage in every position of interest. We developed and built a ring antenna array to fulfill this requirement. It consists of 8 Rx patch antennas placed on the walls of an octagonal prism and a Tx antenna with omnidirectional coverage in azimuth (see Fig. 2). The line-of-sight signal from the target is always received by at least three patch antennas over the complete azimuth range with this arrangement. The setup cannot make any elevation angle measurements, however.

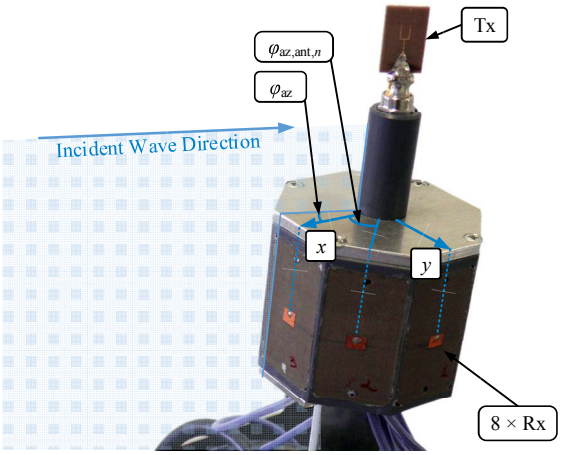

Fig. 2. 8-element ring antenna array with omnidirectional coverage in azimuth.

The model for the peak of the Fourier transform of the mixed-down signal S_n in channel $n = 1…8$ is

$$S_n = A_n \cdot \exp(\phi_{g,n} + \phi_{c,n}), \tag{1}$$

where A_n is the signal amplitude [7]. The phase term $\phi_{g,n}$ describes the phase difference in every channel due to the spatial distribution of the antennas. The term $\phi_{c,n}$ is an error term, which should be removed by calibration.

Given the specific array structure, we use a combination of amplitude-comparison monopulse (AM) and phase-comparison monopulse (PM) techniques to estimate the azimuth angle from the signal in (1). We use AM similar to [8] in a first step to get a rough estimate $\varphi_{az,AM}$ of the real azimuth angle φ_{az}. The received amplitudes A_n are normed to the maximum received amplitude by

$$\overline{A_n} = A_n / \max_n\{A_n\}. \tag{2}$$

We then search through the complete azimuth range $\varphi_{az,h} = -180°...179°$ to find the minimum of the cost function $R(\varphi_{az,h})$:

$$\begin{aligned} R(\varphi_{az,h}) &= \sum_{n=1}^{8} |\,\overline{A_n} - A_{n,h}(\varphi_{az,h})\,|, \\ \varphi_{az,AM} &= \arg\min_{\varphi_{az,h}}\{R(\varphi_{az,h})\}. \end{aligned} \tag{3}$$

The hypothesis for the amplitude $A_{n,h}$ is

$$A_{n,h}(\varphi_{az,h}) = \mathrm{RP}(\mathrm{wrap}(\varphi_{az,ant,n} - \varphi_{az,h})), \tag{4}$$

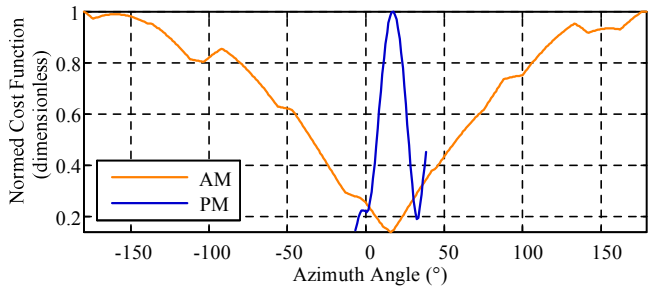

Fig. 3. Amplitude monopulse (AM) and phase monopulse (PM) pseudospectra.

where $\varphi_{\mathrm{az,ant},n}$ is the orientation of antenna n in the array reference frame (cf. Fig. 2). The function "RP" returns the normed amplitude from the antenna radiation pattern corresponding to the angle in its argument. It can also be implemented as a lookup table (LUT) if no analytical expression is available. It simplifies to the cosine function in our case of a patch antenna and variation of the azimuth angle only. The "wrap"-function constrains its argument to the range $[-\pi, \pi)$. The pseudospectrum of the amplitude monopulse applied to a real measurement is shown in orange in Fig. 3.

The result $\varphi_{\mathrm{az,AM}}$ is a stable but coarse estimate. It is useful for identifying the 3 signals $\hat{S}_n$, containing useful phase information, since the remaining channels would typically receive only noise or multipath reflections. The signals $\hat{S}_n$ are then used for PM (delay-and-sum beamforming). The corresponding matched filter H_n with the wave vector $\boldsymbol{k}(\varphi_{\mathrm{az}}, \vartheta_{\mathrm{el}})$ are defined as

$$H_n(\varphi_{\mathrm{az}}, \vartheta_{\mathrm{el}}) = \exp\left(-j\boldsymbol{k}^{\mathrm{T}}(\varphi_{\mathrm{az}}, \vartheta_{\mathrm{el}}) \cdot \boldsymbol{r}_{\mathbf{Rx},n}\right),$$
$$\boldsymbol{k}(\varphi_{\mathrm{az}}, \vartheta_{\mathrm{el}}) = \frac{2\pi}{\lambda} \cdot \begin{pmatrix} \cos\varphi_{\mathrm{az}} \cos\vartheta_{\mathrm{el}} \\ \sin\varphi_{\mathrm{az}} \cos\vartheta_{\mathrm{el}} \\ \sin\vartheta_{\mathrm{el}} \end{pmatrix}. \tag{5}$$

The term $\boldsymbol{r}_{\mathbf{Rx},n}$ is the 3D position of antenna n in the array reference frame, and λ is the signal wavelength. The searched azimuth angle $\varphi_{\mathrm{az,PM}}$ is at the maximum of the cost function $I(\varphi_{\mathrm{az,h}}, \vartheta_{\mathrm{el,h}})$ over the interval $[\varphi_{\mathrm{az,AM}} - \Delta\varphi, \varphi_{\mathrm{az,AM}} + \Delta\varphi]$:

$$I(\varphi_{\mathrm{az,h}}, \vartheta_{\mathrm{el,h}}) = \left| \sum_{n=1}^{3} \hat{S}_n \cdot H_n(\varphi_{\mathrm{az,h}}, \vartheta_{\mathrm{el,h}}) \right|,$$
$$\varphi_{\mathrm{az,PM}} = \underset{\varphi_{\mathrm{az,h}}, \vartheta_{\mathrm{el,h}}}{\arg\max} \{ I(\varphi_{\mathrm{az,h}}, \vartheta_{\mathrm{el,h}}) \}. \tag{6}$$

The search range $\Delta\varphi$ should be chosen carefully – if it is too small, one could miss the peak in the phase monopulse pseudospectrum; if it is too large, one might erroneously detect a high side lobe as the correct result. The resulting pseudospectrum for $\vartheta_{\mathrm{el,h}} = 0°$ is shown in blue in Fig. 3. We can search over $\vartheta_{\mathrm{el,h}}$ as well, as shown in (6). This allows us to estimate the azimuth angle more accurately (despite not being able to measure the elevation angle reliably), since the antenna arrangement is two-dimensional when looked at from $\vartheta_{\mathrm{el}} \neq 0°$.

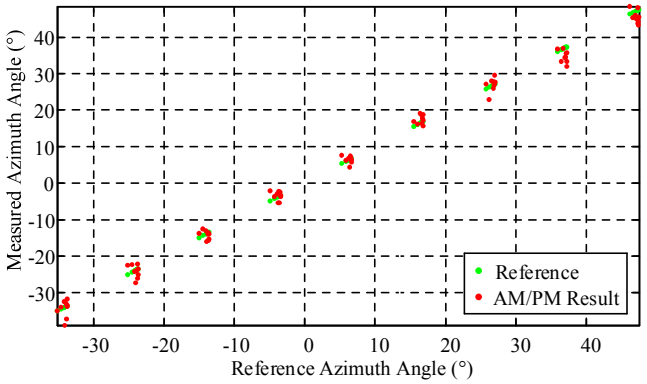

Fig. 4. Azimuth angle measurement result in anechoic chamber for a measurement range of −35° to 50° in azimuth and −40° to 40° in elevation.

The result of a measurement campaign in an anechoic chamber is shown in Fig. 4. One radar node was static and the node with the ring antenna array was rotated in both azimuth direction in the range −35° to 50° and in elevation direction in the range −40° to 40°. We estimate that the RMSE for the azimuth measurement compared to an optical reference is 1.9°.

C. Inclinometer

Only the azimuth angle can be measured using the ring antenna array in Fig. 2. We deploy a Posital Fraba ACS-080 inclinometer as well to determine the complete 3D orientation of the mobile robot. It has two axes with specified measurement range of ±80°, 0.01° resolution and 0.1° accuracy.

IV. Extended Kalman Filter

We use an extended Kalman filter (EKF) to fuse the results of the three sensor types (reference node, mobile node, and inclinometer) [9]. We deliberately refrain from the usage of odometry, so that the proposed solution is generically applicable for all kinds of vehicles (e.g., legged robots).

We define the state vector $\boldsymbol{\mu}$ as

$$\boldsymbol{\mu} = [\boldsymbol{p}_{\mathrm{xyz}}\ \boldsymbol{v}_{\mathrm{xyz}}\ \boldsymbol{\theta}_{\alpha\beta\gamma}\ \boldsymbol{\omega}_{\alpha\beta\gamma}]^{\mathrm{T}}, \tag{7}$$

with the 3D position $\boldsymbol{p}_{\mathrm{xyz}} = [x\ y\ z]$, the 3D translational velocity $\boldsymbol{v}_{\mathrm{xyz}} = [v_{\mathrm{x}}\ v_{\mathrm{y}}\ v_{\mathrm{z}}]$, the 3D orientation $\boldsymbol{\theta}_{\alpha\beta\gamma} = [\alpha\ \beta\ \gamma]$ and the 3D rotational velocity $\boldsymbol{\omega}_{\alpha\beta\gamma} = [\omega_\alpha\ \omega_\beta\ \omega_\gamma]$. All values are defined relative to a static reference frame, which will be denoted as the global frame. The z-axis of the global frame is aligned with gravity. The filter is initialized with a random position $\boldsymbol{p}_{\mathrm{xyz}}$ and orientation $\boldsymbol{\theta}_{\alpha\beta\gamma}$ and a very high uncertainty $\boldsymbol{\sigma}$. The measurements from the reference nodes have the form $\boldsymbol{h}_{\mathrm{ref}} = [d\ \varphi_{\mathrm{az}}\ \vartheta_{\mathrm{el}}]$, with the distance d, azimuth angle φ_{az} and elevation angle ϑ_{el} in the known radar reference frame. Using simple geometric considerations, $\boldsymbol{h}_{\mathrm{ref}}$ is transformed to the global frame to get $\boldsymbol{h}_{\mathrm{ref,glo}}$, i.e. it is converted from measurement space to state space. The measurement matrix $\boldsymbol{H}$ which is the Jacobian of $\boldsymbol{h}_{\mathrm{ref,glo}}$ w.r.t. $\boldsymbol{x}$ is thus trivial to calculate. In order to correctly fuse the measurement uncertainty $\boldsymbol{Q}$, it needs to be transformed to state space using the transformation matrix $\boldsymbol{G}$, where $\boldsymbol{G}$ is the Jacobian of $\boldsymbol{h}_{\mathrm{ref}}$ w.r.t. $\boldsymbol{x}$. The corresponding update of the discrete-time extended Kalman filter is then given by

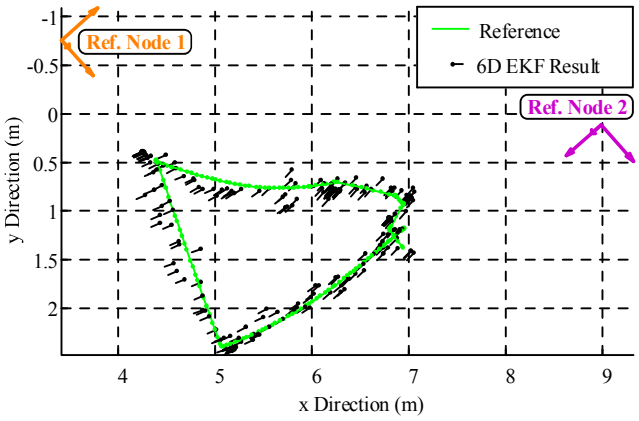

Fig. 5. Measured trajectory in DFKI space exploration hall (top view).

$$\boldsymbol{S} = \boldsymbol{H}\sigma_k\boldsymbol{H}^{\mathrm{T}} + \boldsymbol{G}\boldsymbol{Q}\boldsymbol{G}^{\mathrm{T}}, \boldsymbol{K} = \sigma_k\boldsymbol{H}^{\mathrm{T}}\boldsymbol{S}^{-1},$$
$$\boldsymbol{\mu}_{k+1} = \boldsymbol{\mu}_k + \boldsymbol{K}(\boldsymbol{z} - \overline{\boldsymbol{z}}), \sigma_{k+1} = (\boldsymbol{I} - \boldsymbol{K}\boldsymbol{H})\sigma_k, \quad (8)$$

with the time step index k. The measurement vector (the expected measurement vector) is given by $\boldsymbol{z} = \boldsymbol{h}_{\mathrm{ref,glo}}$ ($\overline{\boldsymbol{z}} = \boldsymbol{p}_{\mathrm{xyz}}$).

The inclinometer output consists of the angles x_{an} and y_{an} between the inclinometer x- and y-axis, respectively, and the xy-plane of the global frame. We convert these angles to the pitch and roll angles β and γ in the global frame using geometric transformations. We can estimate the yaw angle α in the global frame from the geometry based on an estimate of β and γ and an azimuth angle measurement φ_{az} from the mobile node. We perform the conversion of the corresponding measurement uncertainty to state space numerically since the analytical solution contains very long equations. The measurements can then be fused in a manner similar to (8). We implement the EKF propagation step by a simple motion model using the velocities defined in (7). A more in-depth description of the EKF is outside the scope of this paper.

V. Measurement Results

The 6D EKF result of a test in the scenario from Fig. 1 is depicted in Fig. 5. The black dots denote the 3D position and the black lines the 3D orientation of the mobile robot. We moved the robot in one plane in a triangle-like trajectory while keeping its orientation approximately constant. This result demonstrates the very good overall WLN reliability and accuracy. The 3D position RMSE was determined to 13.8 cm and the maximum error was 37.1 cm compared to a high-precision optical tachymeter. We tested the system in a 3D scenario as well: we conducted this second measurement campaign with four reference nodes at Friedrich-Alexander-University Erlangen-Nürnberg (FAU) where the mobile robot started on a table, moved down a ramp and drove around it as shown in Fig. 6. The resulting 3D position RMSE was 16.8 cm and the maximum error 46.8 cm. Unfortunately, no reference was available for the orientation. Nonetheless, the results show that the orientation is also qualitatively

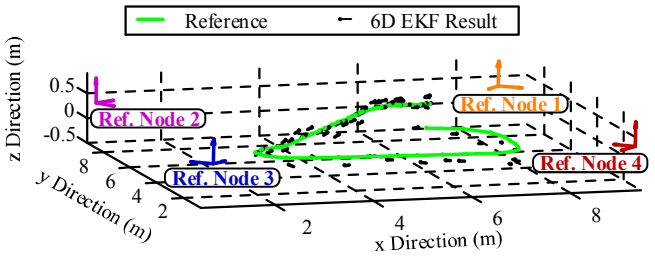

Fig. 6. Measured trajectory at Friedrich-Alexander-University Erlangen-Nürnberg (FAU) (3D view).

correct and stable. The worse accuracy in the second scenario is most likely due to robot positional variations in 3D, multipath reflections at the ramp and higher robot velocity, since the radar measurement rate was very limited in the prototypes used.

VI. Conclusion

We present a wireless localization network for 6D pose estimation of a mobile robot. We successfully verified system accuracy and reliability in two measurement scenarios. Hence, we believe the system can be used to improve localization in space exploration as well as in terrestrial applications. A higher measurement rate could further enhance the system performance and an increase in channel count could improve localization accuracy.

References

[1] M. W. Powell, T. Crockett, J. M. Fox, J. C. Joswig, J. S. Norris, K. J. Rabe, M. McCurdy, and G. Pyrzak, "Targeting and localization for Mars rover operations," in *Proc. 2006 IEEE Int. Conf. of Inf. Reuse and Integration IRI-2006*, pp. 23–27, 2006.

[2] R. U. Sonsalla, F. Cordes, L. Christensen, S. Planthaber, J.C. Albiez, I. Scholz, and F. Kirchner, "Towards a heterogeneous modular robotic team in a logistic chain for extraterrestrial exploration", in *Proc. Int. Symp. on Artificial Intelligence, Robotics and Automation in Space*, Montreal, Canada, 2014.

[3] F. Cordes, C. Oekermann, A. Babu, D. Kuehn, T. Stark, and F. Kirchner, „An active suspension system for a planetary rover", in *Proc. Int. Symp. on Artificial Intelligence, Robotics and Automation in Space*, Montreal, Canada, 2014.

[4] S. Roehr, P. Gulden, and M. Vossiek, "Precise distance and velocity measurement for real time locating in multipath environments using a frequency-modulated continuous-wave secondary radar approach," IEEE Trans. Microw. Theory Tech., vol. 56, no. 10, pp. 2329–2339, Oct. 2008.

[5] C. Reustle, D. Shmakov, and M. Vossiek, "A 24 GHz SIMO radar tachymeter for precise transponder localization," in *2015 IEEE MTT-S Int. Microwave Symp.*, 2015, pp. 1–4.

[6] M. Vossiek, L. Wiebking, P. Gulden, J. Wieghardt, C. Hoffmann, and P. Heide, "Wireless local positioning," *IEEE Microw. Mag.*, vol. 4, no. 4 SPEC. ISS., pp. 77–86, 2003.

[7] Y. Dobrev, D. Shmakov, and M. Vossiek, "A Bilateral 24 GHz wireless positioning system for 3D real-time localization of people and mobile robots," in *Proc. 2015 IEEE MTT-S Int. Conf. on Microwaves for Intelligent Mobility (ICMIM)*, 2015, pp. 1–4.

[8] W. Kederer and J. Detlefsen, "Direction of arrival (DOA) determination based on monopulse concepts," in *2000 Asia-Pacific Microwave Conf. Proc. (Cat. No.00TH8522)*, 2000, pp. 1–4.

[9] S. Thrun, W. Burgard, and D. Fox, *Probabilistic robotics*. MA: MIT Press, 2006.